CHAPTER 4.2

Cyclones

Brian Flintoff and Brian Knorr

Cyclones, which are named for the spiraling motion within the body of the device, are one of a large number of classification devices aimed at separating fine particles in a fluid (water or air; e.g., see Kelly and Spottiswood 1982, Svarovsky 2000, or Aldrich 2015 for additional information on this topic). Unfortunately, the seminal work on this subject (Bradley 1965) is now out of print, although occasionally, copies are available. Cyclone classification is generally reserved for the separation of particles on the basis of size. For that reason, other applications for cyclones, such as thickening and dense-medium separation, are not considered here. Broadly speaking, cyclone classifiers can either treat dry feeds (e.g., the air classifier or air separator) or wet/slurry feeds (e.g., the hydrocyclone). Again, as this is a reference source for mineral processing engineers, the emphasis here is on wet applications, and specifically the hydrocyclone.

Unlike the vibrating screen, which employs a physical means (i.e., the screen media) to effect a separation, the cyclone classifier uses differential settling properties of particles of different mass. The cyclonic action within the body of the device develops g-forces significantly greater than gravity, which accelerate the separation process. In general, cyclones are robust, compact (i.e., having a small footprint), and relatively efficient size separation devices.

Figure 1 shows the most common applications of wet cyclones in mining applications. Air classifiers are also commonly used in these applications, for example, as size control devices in dry grinding (most notably in refractory gold, coal-fired power plant pulverizers, or cement clinker applications) and as sorters, usually in dedusting applications.

Figure 2 shows the geometry and key design components of a hydrocyclone, and it is clear from the shape that it resembles the natural phenomena that give rise to the name. The separator comprises a feed section, cylindroconical section, discharge spigot or apex, vortex finder, and overflow. In some cases, usually for larger diameters, each of the components is supplied as a separate entity, whereas in smaller sizes, they may be cast into a single unit. The capacity of a hydrocyclone is a function of its size and, subject to operational constraints, the rate and solids concentration at which the feed (i.e., slurry) material is supplied. In some cases, hydrocyclones are gravity fed from surge tanks, but the majority of applications utilize a feed sump and pump arrangement. Consequently, it is common to use a group of hydrocyclones operating in parallel to achieve the required process capacity. As Figure 3 shows, the compact design of the units permits the use of a radial header to distribute feed to many hydrocyclones. (This is commonly called a *hydrocyclone cluster* or *battery* or *cyclopac*.) Moreover, as the side view highlights, the use of knife-gate valves to open or close a hydrocyclone is very convenient, both from an online process control point of view as well as

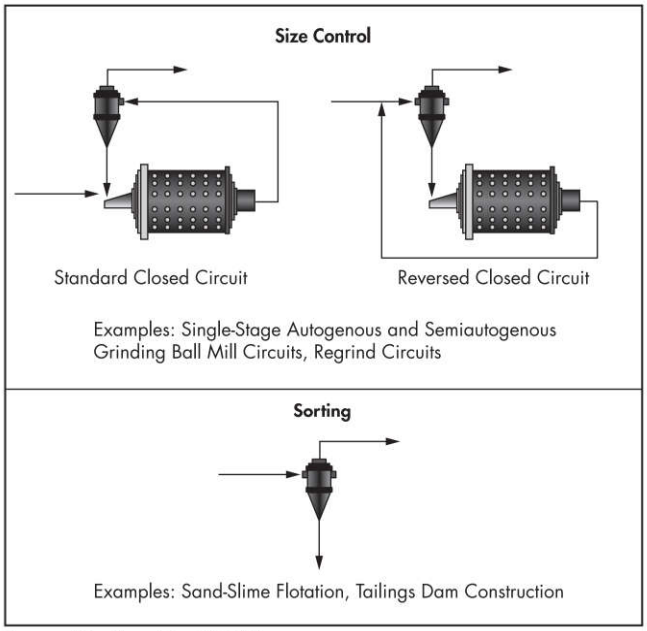

Source: Flintoff and Kuehl 2011

Figure 1 Examples of application classes for hydrocyclones in mining

Brian Flintoff, Consultant, Sigmation Inc., Kelowna, British Columbia, Canada
Brian Knorr, Director, Research & Development, Metso Minerals Industries Inc., York, Pennsylvania, USA

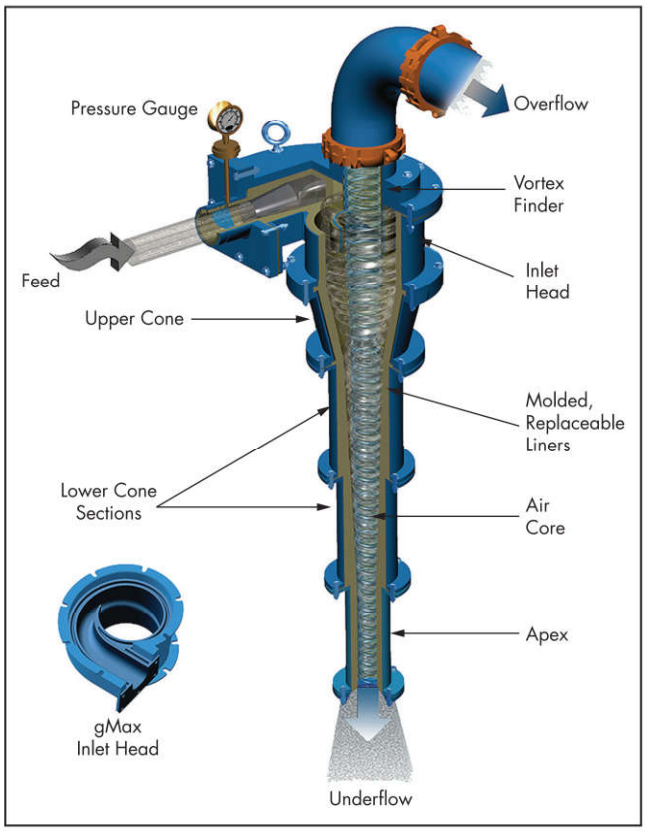

Courtesy of FLSmidth–Krebs

Figure 2 Hydrocyclone design and components

for maintenance purposes. On the latter point, it is typical to design the hydrocyclone cluster with standby hydrocyclone units to allow for removal of a hydrocyclone for maintenance and replacement with a refurbished spare while maintaining operation of the overall hydrocyclone cluster. This is important because the maintenance interval for the hydrocyclone does not typically align with the shutdown schedule of the overall plant.

There are many variants on the more typical hydrocyclone geometry. Figure 4 shows the water-only or automedium cyclone that is frequently used in washing fine (–0.6 mm) coal. (The truncated lower cone section is employed to set up a secondary density separation in a rotating particle bed.) The flat-bottomed hydrocyclone occasionally used in mineral processing applications has a very similar kind of body geometry.

Air separators tend to be designed to treat the whole feed flow, so they are larger units, as shown in Figure 5. These devices can be either static (like the hydrocyclone) or dynamic (include moving blades, etc., to enhance separation).

Figure 5 illustrates a typical dry grinding circuit with the air separator used for classification and a cyclone used for solids recovery. The cutaway view illustrates the internals and the drive for this dynamic air separator.

HYDROCYCLONE BASICS

From about 1950 through 1970, the hydrocyclone evolved into its current role in mineral processing, by which time it had become a key element in the design of most large-scale grinding circuits, offering high capacities in small footprints and arguably enabling the ongoing development of very large grinding circuits. Although they still have their place, mechanical (spiral or screw, rake, etc.) classifiers were effectively rendered obsolete in plant design by the hydrocyclone. Despite the numerous benefits of hydrocyclones, there have always been issues with efficiency. As today's operators look for ways to address energy efficiency, and as competitive technologies emerge, hydrocyclone manufacturers have redoubled their development efforts. As is the case for screens, they are using the very latest simulation tools to help refine existing designs and develop new ones for specific applications, with good success. The following material provides a refresher on hydrocyclone basics and introduces some of the latest tools and techniques for the design, analysis, control, and optimization of hydrocyclones.

Principles of Operation

Figure 6 offers a sketch of a typical hydrocyclone and the main design components. The principal dimensional variable is the diameter of the upper cylindrical section of the hydrocyclone

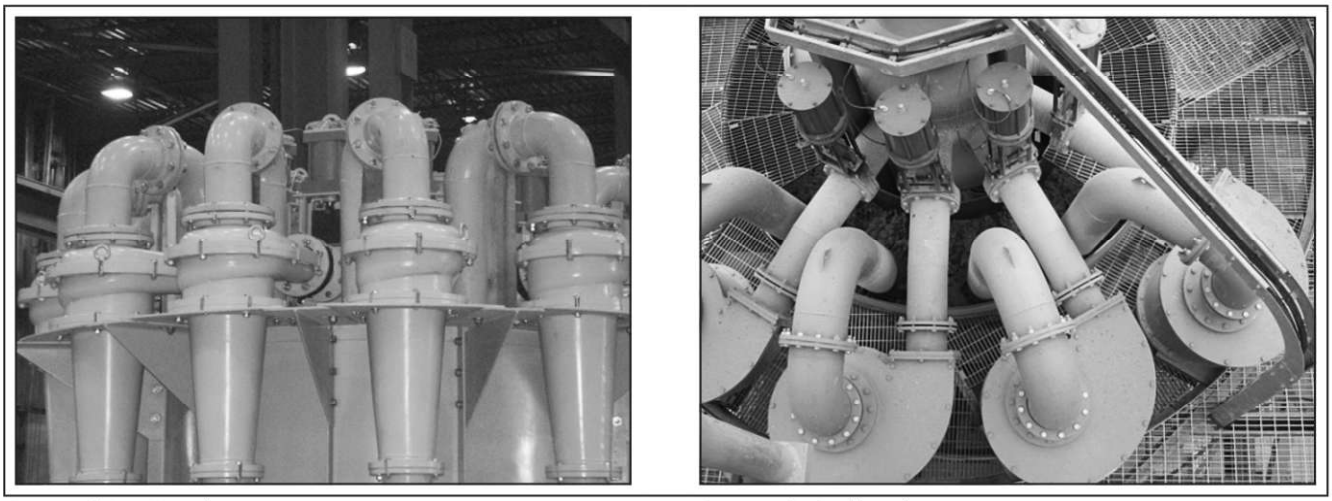

Courtesy of Weir Minerals

Courtesy of FLSmidth–Krebs

Figure 3 Side and top views of hydrocyclone clusters

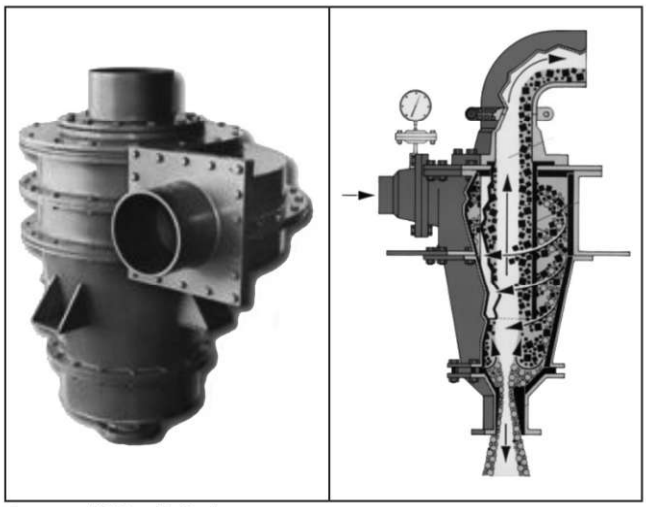

Courtesy of FLSmidth–Krebs

Figure 4 Water-only cyclone

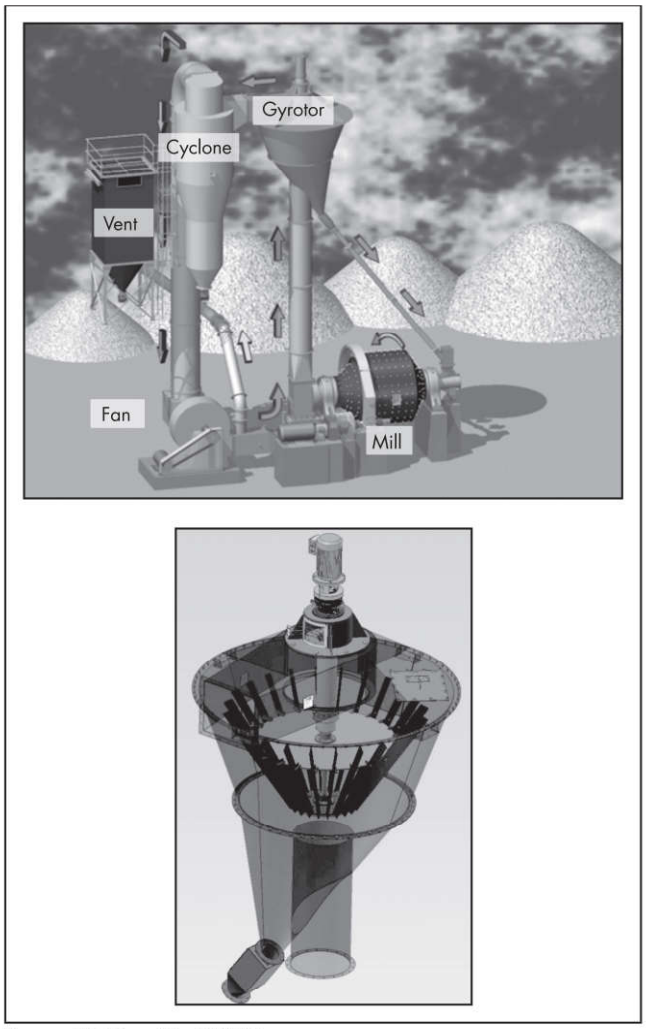

Source: Flintoff and Kuehl 2011

Figure 5 Gyrotor air separator in a typical dry grinding circuit

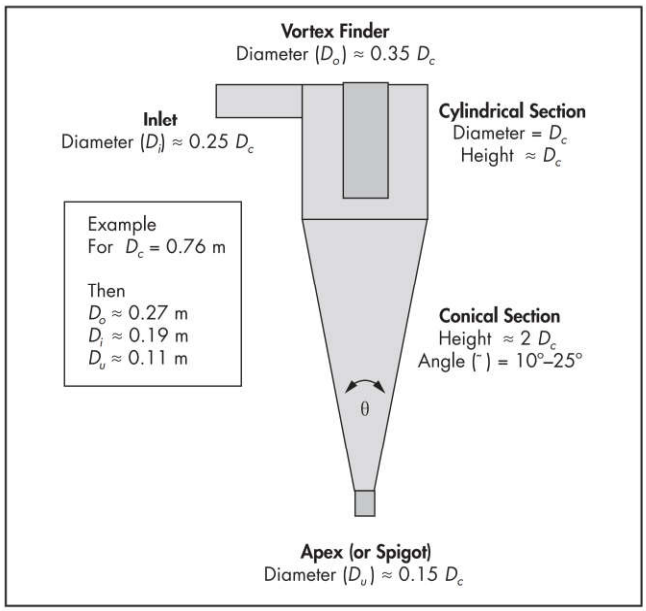

Figure 6 Principal design elements of a hydrocyclone

body, D_c. The inlet (D_i) and discharge (D_o and D_u) dimensions usually lie within some ratio of D_c, for example, $0.2D_c \leq D_o \leq 0.45D_c$. Because the inlet is usually more rectangular, to facilitate a reduction in turbulence on entry (i.e., involute designs; see Olson and Turner 2002 or Aldrich 2015 for examples), D_i is the diameter of a circle with an area equivalent to the actual inlet area. In the past, smaller hydrocyclones have had lower cone angles (~10°), but because of headroom considerations, larger hydrocyclones tend to have larger cone angles (~20°). Depending on the application requirements, some large hydrocyclones have dual cone angles, as this has been found to yield finer cut size ($d50c$) values. Some typical dimensions for a hydrocyclone with D_c = 76 cm are shown in the figure.

The feed enters the hydrocyclone near the top of the cylindrical section, usually through some sort of involute inlet design (see Olson and Turner 2002 or Aldrich 2015 for examples). In the newer hydrocyclone designs, the involute is ramped, which is intended to introduce the slurry into the hydrocyclone with a minimum of turbulence, as this can have a deleterious effect on efficiency and wear. (The top view in Figure 3 clearly shows an involute design.) The rotational motion set up in the body of the hydrocyclone gives rise to the g-forces that accelerate the particle separation process. All of the particles are subjected to the centrifugal forces directing them to the wall of the hydrocyclone, where this material moves downward in a helical fashion to be discharged through the apex, *as underflow*. However, as the particles migrate to the outer wall of the hydrocyclone, they necessarily displace the fluid, which must move inward. The fluid exerts drag forces on the particles and retards their outward motion and, in the case of the finer particles, actually causes them to move inward. This stream moves upward in a helical path to be discharged through the vortex finder, *as overflow*. When the hydrocyclone is operating normally, the centrifugal forces acting on the slurry create low pressure along the central axis, establishing the conditions necessary for development of the characteristic air core.

To look a little more closely at the separation process, consider Stokes' law for laminar settling, given by Equation 1. (Whether it is Stokes' law, Newton's law, or something else—as experimental data would seem to indicate—the trends predicted by Stokes' law are seen in practice.)

$$v_t = \frac{(\rho_s - \rho_l) G d^2}{18\mu} \qquad \textbf{(EQ 1)}$$

where

v_t = terminal settling velocity
ρ_s = solids density
ρ_l = carrier fluid density
G = g-force
d = particle diameter
μ = carrier fluid viscosity

From the preceding explanation, anything that acts to increase the particle settling velocity increases the chances of the particle reporting to the underflow stream. Clearly, the larger the particle, the more likely it is to go to the underflow. Similarly, higher g-forces (meaning higher feed flows or pressure drops with the resulting increased velocities inside the hydrocyclone) will also act to increase the probability that a particle will find its way to the underflow stream. Particles with higher density will also have a higher probability of reaching the underflow stream.

However, if the feed material contains a lot of very fine clay material, thereby increasing the effective viscosity, the particles will be less likely to reach the underflow stream. Similarly, with high-density hydrocyclone feeds, there is a significant concentration of fine particles in the carrier fluid, which increases the fluid density and makes it less likely for particles to reach the underflow stream.

To further complicate things, the size of the vortex finder also has an influence on the separation outcome. Smaller vortex finders will create a finer particle overflow stream, and vice versa. To a lesser extent, the apex size will also have an impact, as a smaller apex tends to limit the underflow capacity. This results in a diversion of some coarser particles toward the upper regions of the hydrocyclone, the finest of which will then be entrained in the overflow stream.

Figure 7 (absent the air core) was developed by Renner and Cohen (1978) and roughly shows the main regions inside a hydrocyclone. Region A is a relatively narrow area in the vicinity of the inlet that is characterized by a size distribution similar to that of the feed. Region B is the finer material with a size distribution very similar to the overflow product. Region C is perhaps the most critical area, as it contains significant quantities of near-size particles, which suggests that they tend to accumulate here until physical capacity constraints force them to move to one product zone or the other. Arguably, this is the region of active classification, and poor operation would be expected if it fails to form properly, possibly because of poor design, excessive feed solids concentrations, or some other reason. Most of the conical section is region D, characterized by a coarser size distribution similar to the underflow.

Rather than produce a process matrix for the hydrocyclone, the authors have chosen to illustrate these concepts with the Plitt model (adapted from Flintoff et al. 1987) given in Equation 2. This is the correlation for the corrected cut size, $d50c$. For example, increasing the hydrocyclone, D_c, or vortex finder diameter, D_o, or percent solids in the feed would be expected to lead to a coarser cut size. Similarly, increasing the feed flow, Q, or particle density, ρ_s, would lead to a finer cut size.

$$d50c = \frac{C D_c^{0.46} D_i^{0.6} D_o^{1.21} \mu^{0.5} e^{0.063V}}{D_u^{0.71} h^{0.28} Q^{0.48} \left(\frac{\rho_s - \rho_l}{1.65}\right)^k} \qquad \textbf{(EQ 2)}$$

where

$d50c$ = corrected cut size
C = calibration constant
D_c = hydrocyclone diameter
D_i = inlet diameter
D_o = vortex finder diameter
V = volume percent concentration of solids in hydrocyclone feed
D_u = apex diameter
h = free vortex height (distance from bottom of vortex finder to top of apex)
Q = feed volumetric flow rate
k = settling exponent (theoretically 0.5 for laminar setting and 1 for turbulent setting)

As Equation 11 in Chapter 4.6, "Partition Curves," indicates, $d50c$ is just one of the parameters in the usual partition curve models, yet it is very strongly correlated with the hydrocyclone overflow particle size as shown in Figure 8. Consequently, one can use $d50c$ as a proxy for overflow size when contemplating design or operational changes to influence performance.

Before leaving this section, there are a few operating situations worthy of some amplification. The first is the condition known as *roping* (a name based on the appearance of the underflow stream in this regime). Roping occurs when the volumetric flow rate of the underflow stream increases to the point where it causes the air core to collapse. When this happens, the usual helical spray from the apex alters appearance, as shown in Figure 9. Consequently, roping can and eventually will increase the flow of coarser particles to the overflow stream, that is, a coarser cut size. The impact on efficiency (as measured by α in a partition curve) appears to depend on the hydrocyclone feed density, with higher densities having

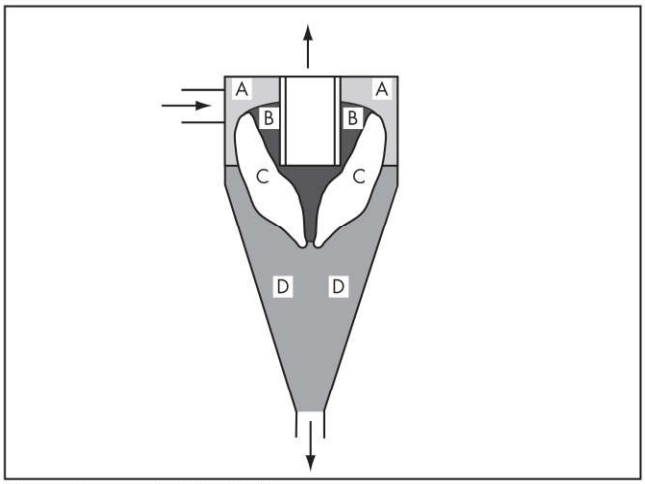

Source: Renner and Cohen 1978
Figure 7 Regions in a hydrocyclone

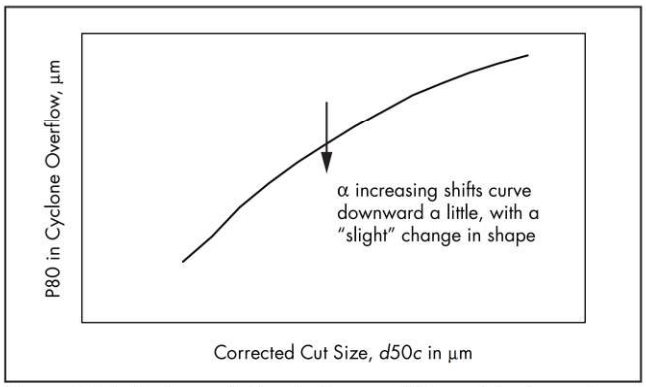

Figure 8 Typical correlation between *d50c* and hydrocyclone overflow particle size (here measured as P80)

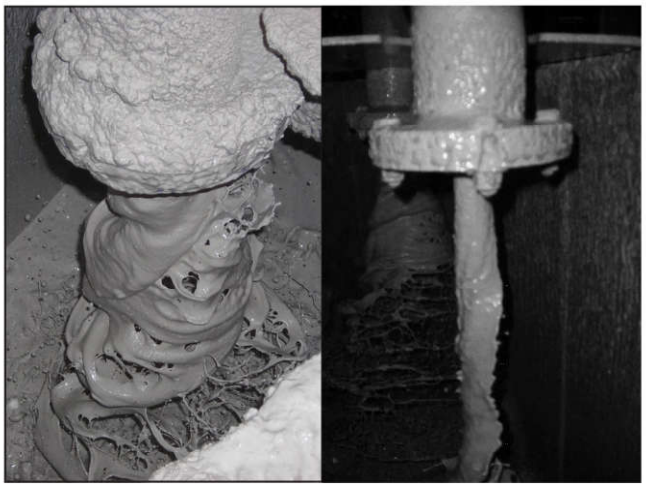

Courtesy of Metso

Figure 9 Spray and rope discharge

a more deleterious effect (see Plitt et al. 1987). Roping does tend to maximize the underflow density, and thus minimizes the fraction of fine material that reports with the carrier liquid to this stream. Figure 10 shows a comparison of partition curves in spray and open discharge operation. In this instance, the sharpness of separation (α) is seen to increase in the roping mode of operation.

The second operating situation is *surging*. With the increased use of variable-speed pumping and the ability to automatically open and close hydrocyclones, this is not the issue it once was. Nevertheless, it can still happen, and with fixed-speed hydrocyclone feed pumps, this usually necessitates a sheave change. Figure 11 shows a before-and-after case where the hydrocyclone overflow particle size was monitored over approximately 24 hours (sampling every 15 minutes), and the impact of the sheave change on the stability of the particle size trajectory is quite obvious.

The last item of interest is hydrocyclone *mounting*. With the development of larger and larger hydrocyclones, mounting them in a vertical orientation puts a significant head on the underflow stream, which can influence both wear and separation performance (e.g., higher *Rf*). However, tilting these hydrocyclones (usually at ~45°) allows operation at lower pressures while still producing a good underflow product, albeit at a coarser cut size. Maintenance savings claims for wear in the lower region of the hydrocyclone are impressive (e.g., 80%; Schmidt and Turner 1993), but it can be more difficult to perform in situ maintenance for this kind of installation. For the interested reader, Asomah and Napier-Munn (1997) have taken a more quantitative look at the impact of mounting angle on hydrocyclone performance.

HYDROCYCLONE SELECTION

The selection of hydrocyclones is normally a task best performed with the supplier, as these firms possess the knowledge, expertise, databases, and tools to ensure that the best results are achieved. In most cases, it is possible to avoid pilot testing; however, there are some instances where this is preferable and even inevitable. One of the more challenging design problems is the closed-circuit grinding application, illustrated in Figure 1 as *size control*. This is challenging because the hydrocyclone feed characteristics very much depend on mill performance, which in turn depends on the hydrocyclone underflow characteristics, which in turn depend on the feed. Experience has given most suppliers a very good understanding of this problem; nevertheless, circuit simulation tools can be useful adjuncts in developing a hydrocyclone design basis. (The use of empirical hydrocyclone models for design decision

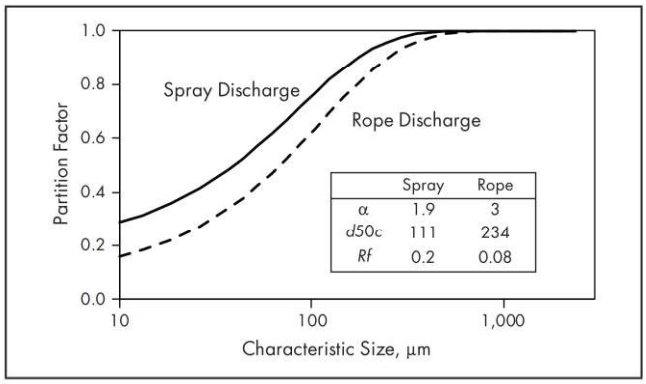

Data from Plitt et al. 1987

Figure 10 Partition curve examples for a hydrocyclone operating in spray and rope discharge modes

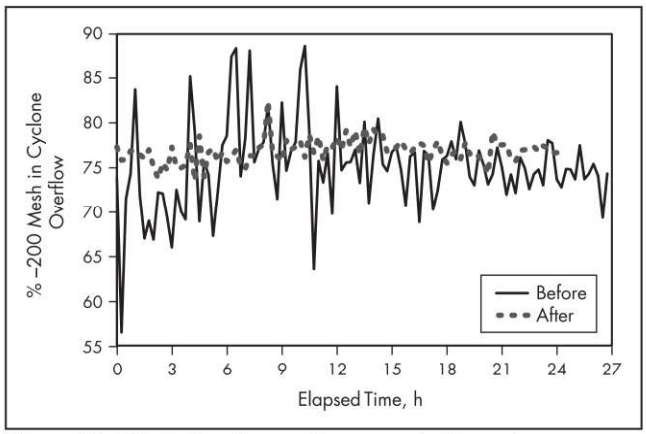

Figure 11 Effect of a sheave change on hydrocyclone performance as measured by hydrocyclone overflow particle size

support is discussed later in the "Hydrocyclone Modeling and Simulation" section.)

The techniques of hydrocyclone selection applicable to older hydrocyclone geometries (for more detail, see Arterburn 1982 and/or Olson and Turner 2002) are briefly reviewed in this section. Although the authors have questioned their current applicability with the leading hydrocyclone original equipment manufacturers (OEMs), the feedback is that these methods are still in use. The newer hydrocyclone geometries, however, require additional correction factors, but these are proprietary to the OEMs. On this basis, the following illustrative example is applicable to older hydrocyclone geometries.

The required information for hydrocyclone selection is summarized in Figure 12. A set of standard tests under very specific design and operating conditions was performed to develop a relationship between what is called the *base corrected cut size* ($d50c_{base}$) and the principal dimensional variable, the hydrocyclone diameter, D_c. The outcome of this work is captured in Figure 13, based on Equation 3a, also given in the alternate form as Equation 3b:

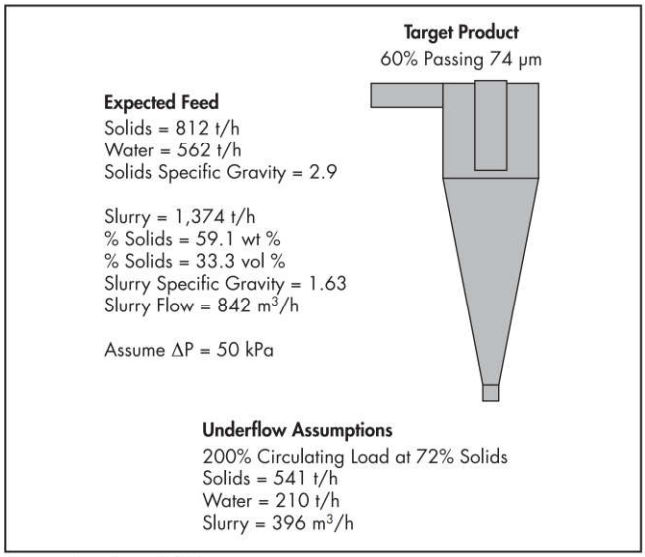

Source: Arterburn 1982

Figure 12 Hydrocyclone design

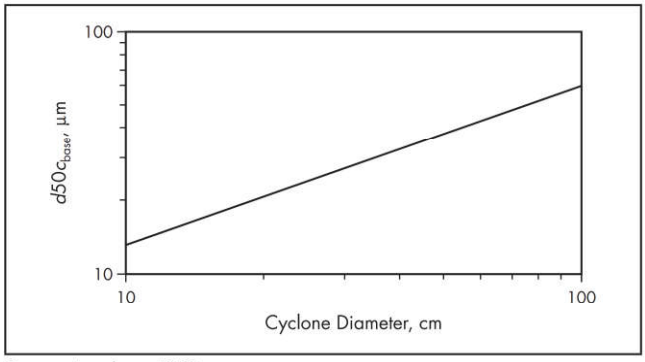

Source: Arterburn 1982

Figure 13 $d50c_{base}$ versus hydrocyclone diameter for standard hydrocyclones

$$d50c_{base} = 2.84D_c^{0.66} \quad \textbf{(EQ 3a)}$$

$$D_c = 0.206d50c_{base}^{1.515} \quad \textbf{(EQ 3b)}$$

The hydrocyclone design approach illustrated here relies on many empirical correction factors to scale the performance of the standard hydrocyclone to the expected industrial operation. In this case, the key scaling parameter is the $d50c$, and the key design formula is given by Equation 4a:

$$d50c_{actual} = d50c_{base}(CP1)(CP2)(CP3)(\ldots)(CD1)(CD2)(CD3)(\ldots) \quad \textbf{(EQ 4a)}$$

where

$d50c_{actual}$ = expected corrected cut size in industrial operation
$d50c_{base}$ = corrected cut size for the standard hydrocyclone
CP = process-related correction factors, for example, feed volume (approximate viscosity) correction factor
CD = design-based correction factors, for example, vortex finder diameter

In practice, Equation 4a is rearranged and used in the following form:

$$d50c_{base} = \frac{d50c_{actual}}{(CP1)(CP2)(CP3)(\ldots)(CD1)(CD2)(CD3)(\ldots)} \quad \textbf{(EQ 4b)}$$

With this short introduction, the four basic steps in hydrocyclone design are discussed next.

Step 1. Estimate $d50c_{actual}$

Table 1 provides the relationship between the overflow size specification and $d50c_{actual}$. For the overflow specification in Figure 12, 60% corresponds to a factor of 2.08 that when multiplied by the reference size of 74 µm gives the estimate for $d50c_{actual}$ of 154 µm.

Step 2. Calculate Correction Factors and Estimate $d50c_{base}$

There are three important published process-related correction factors: solids feed volume concentration, operating pressure drop, and solids specific gravity.

Table 1 Empirical correlation between the reference size and $d50c_{actual}$

Required Overflow Size Distribution (% passing of specified µm size)	Multiplier (used to factor the specified size)
98.8	0.54
95	0.73
90	0.91
80	1.25
70	1.67
60	2.08
50	2.78

Source: Arterburn 1982

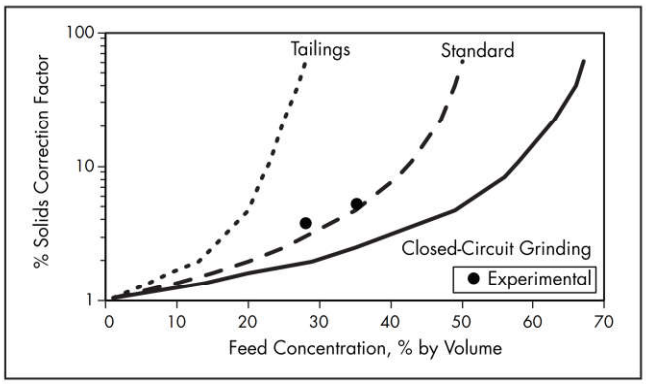

Adapted from Olson and Turner 2002

Figure 14 Correction factors (*CP*1) for hydrocyclone feed solids volumetric concentration

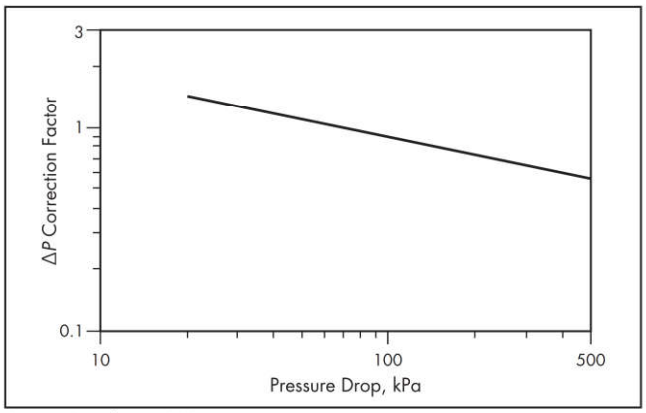

Source: Arterburn 1982

Figure 15 Pressure drop correction factor (*CP*2)

*CP*1 is the correction for the feed volumetric concentration, which is, in effect, a first-order approximation to viscosity. Of course, viscosity also depends on water temperature, clay concentrations, particle shape, and other factors; clays in fine tailings are what gave rise to the tailings curve in Figure 14. In this figure, Olson and Turner (2002) extended Arterburn's method (which was based on the standard curve in Equation 5).

In Chapter 4.6, "Partition Curves," two hydrocyclone sampling experiments are described. With the data from these experiments, it was possible tto back calculate the *CP*1 factor values: These two points appear to fall on the standard curve in Figure 14 and not the closed-circuit curve, as might have been expected. When to use which curve is the purview of the OEM, hence the suggestion to consult it in hydrocyclone design studies.

$$CP1 = \left[\frac{53 - V}{53}\right]^{-1.43} \quad \textbf{(EQ 5)}$$

In this example, we assume the standard curve, and with V = 33.3%, then $CP1 = 4.09$.

*CP*2 is the correction factor for the operating pressure drop, which is usually the difference between the measured pressure in the radial header and atmosphere. Larger hydrocyclones tend to run at lower pressures and vice versa. Figure 15 and Equation 6 show this relationship.

$$CP2 = 3.27\Delta P^{-0.28} \quad \textbf{(EQ 6)}$$

where ΔP is the pressure drop, in kilopascals. In this example, we assume ΔP = 50 kPa, which should give relatively good hydrocyclone performance while minimizing wear. From Equation 6, $CP2 = 1.09$.

*CP*3 is the correction factor for the solids specific gravity and is shown in Figure 16 and Equation 7. For a solids specific gravity of 2.9, the correction factor $CP3 = 0.93$.

$$CP3 = \left[\frac{1.65}{\rho_s - \rho_l}\right]^{0.5} \quad \textbf{(EQ 7)}$$

*CD*1 is the correction factor for the vortex finder diameter. In this example, the default design of $D_o = 0.3D_c$ is used ($CD1 = 1$), and Figure 17 and Equation 8 illustrate the nature of the correction.

$$CD1 = \left[\frac{D_o}{0.3D_c}\right]^{0.6} \quad \textbf{(EQ 8)}$$

Given the correction factors, Equation 4b solves as

$$d50c_{\text{base}} = \frac{154\ \mu\text{m}}{(4.09)(1.09)(0.93)(1)} = 37\ \mu\text{m} \quad \textbf{(EQ 9)}$$

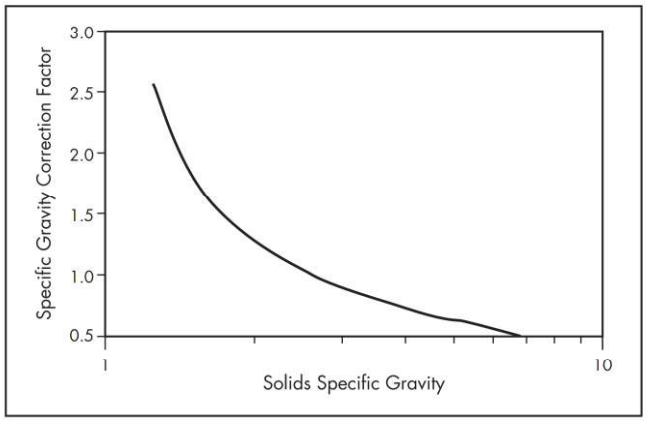

Source: Arterburn 1982

Figure 16 Solids specific gravity correction factor (*CP*3)

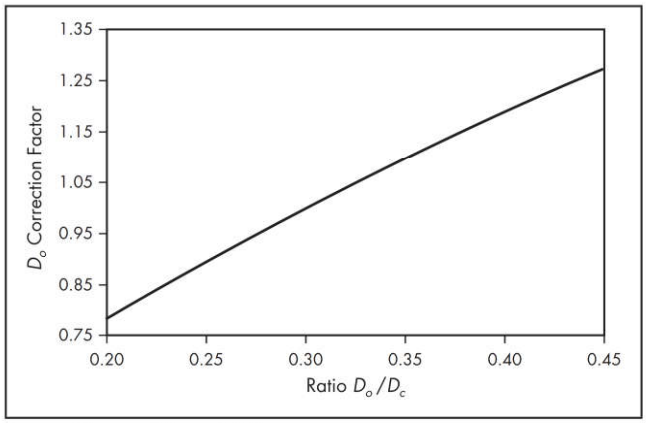

Source: Olson and Turner 2002

Figure 17 Vortex finder correction factor (*CD*1)

Step 3. Select Size and Number of Hydrocyclones

From Equation 4b or Figure 13, the diameter of the hydrocyclone required to give this $d50c_{base}$ is 49.1 cm. Hydrocyclones, like screens, come in certain standard sizes, usually defined by D_c. As shown in Figure 18, the closest size to the *theoretical* value computed earlier is a hydrocyclone with D_c = 51 cm.

From Figure 18, for a pressure drop of 50 kPa, the capacity of a single 51-cm hydrocyclone will be approximately 140 m^3/h. From Figure 12, the total feed volumetric flow is 842 m^3/h, so approximately six hydrocyclones will be required in operation. In practice, two or three additional hydrocyclones would be added to accommodate maintenance as well as peaks in the feed flow rate. It is also not uncommon to provide an additional offtake valve in the radial header to be used for sample collection purposes.

Step 4. Select Apex Size

The last step is to determine the apex size, and that comes from Figure 19. For a total underflow flow rate of 396 m^3/h, the flow through each apex would be ~66 m^3/h, corresponding to an apex size of ~9.3 cm. The manufacturer's closest size would be chosen, if possible tending to a smaller size in anticipation of wear.

Of course, once the hydrocyclones are installed and in operation, the reality of the application is known and the optimization process (process variables and design variables such as D_o and D_u) can be modified as required.

HYDROCYCLONE PERFORMANCE ASSESSMENT

Hydrocyclone performance is usually assessed through the partition curve and related efficiency metrics, and this subject is covered in some detail in Chapter 4.6, "Partition Curves."

HYDROCYCLONE MODELING AND SIMULATION

With the advent of mathematical modeling of tumbling mills (also called *population balance modeling*) in the middle to late 1960s, there was a corresponding need to develop hydrocyclone models that would then permit circuit simulations for process analysis, optimization, and design purposes. Research on the mathematical models of hydrocyclones was arguably most prominent from the 1960s to 1980s but continues to this day with both refinements to existing models and development of new models aimed at providing more robust predictions.

Many researchers have contributed to the field of hydrocyclone modeling. A majority of the success has been in the development and application of empirical models. Most notably, the two empirical models in greatest use today are those of Plitt (see Flintoff et al. 1987) and Nageswararao (see Nageswararao et al. 2004). These models have been incorporated into some of the more common mineral-processing simulation packages. The most widely used crushing and grinding process simulation software today employs the Nageswararao model. Additional contributions in empirical modeling have been made by Asomah and Napier-Munn (1997) and Narasimha et al. (2014), but these enhancements have not yet evolved into common usage. The Narasimha et al. work has generally been aimed at extending the Nageswararao model.

In contrast to the history of these empirical models, there has been limited success to date in more theoretical or phenomenological models. This dominance by empirical models is primarily a result of the complex conditions inside an operating hydrocyclone (e.g., hindered settling, viscosity effects). These material-specific complexities introduce significant challenges for theoretical and phenomenological model developers and will be briefly discussed in the next section.

As with all unit operation model development, two separate uses need to be considered for hydrocyclone models: (1) simulation of existing installations for plant optimization and (2) simulation for greenfield plant design. Once calibrated with survey data from an existing plant operation, the empirical hydrocyclone models show strength in providing

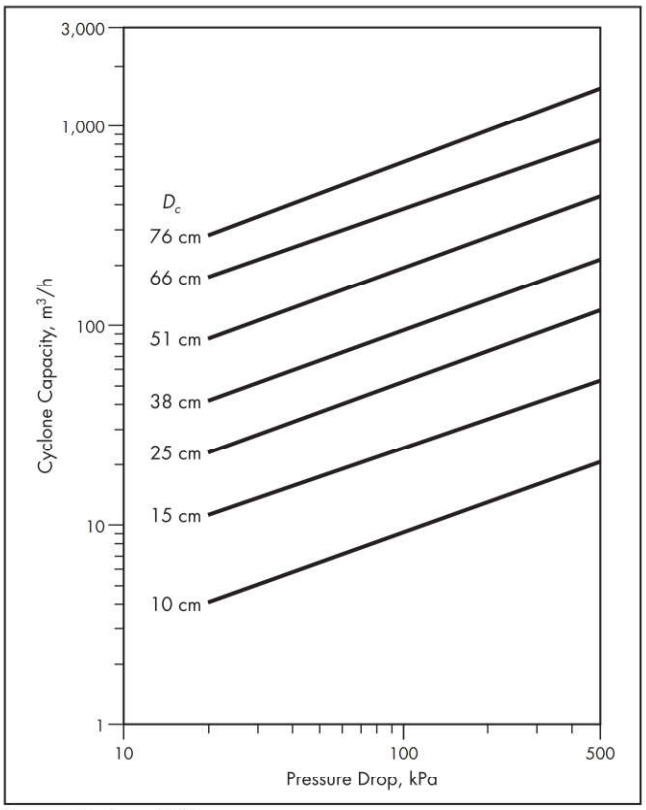

Source: Arterburn 1982

Figure 18 Hydrocyclone capacity correlation

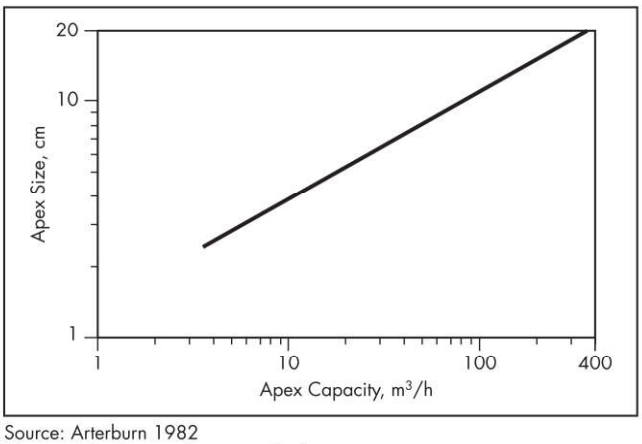

Source: Arterburn 1982

Figure 19 Apex size correlation

predictions for changes in operating conditions and/or hydrocyclone fitting sizes (e.g., vortex finder and apex diameter) in that specific installation. Where the current empirical models are less reliable is in greenfield process predictions and equipment selection. For this reason, and as noted previously, readers are recommended to consult with the equipment suppliers having specific expertise in hydrocyclone selection.

Model Development

To provide a comprehensive prediction of performance, the three primary requirements for any hydrocyclone model are as follows:

1. Predicting the corrected partition curve ($d50c$ and α)
2. Predicting the feed water split to the underflow (Rf)
3. Defining the relationship between feed flow rate and operating pressure ($P \propto Q$)

Partition Curve

The partition curve tool is the current standard for the analysis and modeling of physical separation systems. (In this chapter, the partition curve defines the solids split by size to the underflow, whereas in the more recent literature on the Nageswararao model, the partition to the overflow is considered. For consistency purposes, the authors use the former definition.) For the purposes of calculating the solids and water splits around a hydrocyclone, the empirical models are essentially a series of correlations involving design and operating variables, which provide estimates of $d50c$, α, and Rf, as well as P. These first three parameters uniquely define the partition curve for homogeneous (dominated by particles of the same specific gravity) ores.

Feed Flow Rate and Operating Pressure

A relationship must be defined between the feed flow rate and operating pressure. This is instrumental toward understanding the practical capacity of the hydrocyclone as well as determining the effects of operating pressure and/or feed flow rate on hydrocyclone performance.

Nageswararao Model

The standard model nomenclature is summarized in Table 2. Figure 20 provides some explanation for the geometrical variables that characterize the hydrocyclone geometry.

The correlations and auxiliary equations that collectively comprise the Nageswararao model are as follows (JKTech 2014):

- The Euler number, EU, is defined as $Q/\left(D_c^{\,2}\sqrt{P/\rho_p}\right)$.
- The dimensionless cut size is defined as $d50c/D_c$.
- The recovery of water to underflow is Rf.
- The volumetric recovery of feed slurry to underflow is R_v.
- Derived from survey data, α is assumed to be a constant.

The following four equations define these dependent variables within the Nageswararao model:

$$\frac{Q}{D_c^{\,2}\sqrt{P/\rho_p}} = K_{Q_o}\left\{D_c^{-0.10}\right\}\left(\frac{D_o}{D_c}\right)^{0.68}\left(\frac{D_i}{D_c}\right)^{0.45}\left(\frac{L_c}{D_c}\right)^{0.20}\theta^{-0.10} \quad \textbf{(EQ 10)}$$

$$\frac{d50c}{D_c} = K_{D_o}\left\{D_c^{-0.65}\right\}\left(\frac{D_o}{D_c}\right)^{0.52}\left(\frac{D_u}{D_c}\right)^{-0.47}\left(\frac{D_i}{D_c}\right)^{-0.50}\left(\frac{L_c}{D_c}\right)^{0.20}\theta^{0.15}\left(\frac{P}{\rho_p g D_c}\right)^{-0.22}\lambda^{0.93} \quad \textbf{(EQ 11)}$$

Table 2 Nageswararao hydrocyclone model symbology

Nomenclature	Description
C_v	Volumetric fraction of cyclone feed solids (0–1)
$d50c$	Corrected classification size, μm
D_c	Diameter of the cyclone, cm
d_i	Mean size of the particles in size class i, μm
D_i	Equal area equivalent diameter of the inlet, cm
D_o	Diameter of the vortex finder, cm
D_u	Diameter of the apex (spigot), cm
EU	Euler number
G	Acceleration due to gravity m/s^2
K_{Qo}, K_{Do}, K_{Wo}, K_{Vo}	Material-dependent constants
L_c	Length of the cylindrical section of the cyclone, cm
P	Cyclone feed pressure, kPa
p_i	Partition factor (percent reporting to underflow) for size class i
Q	Cyclone feed volumetric flow rate, L/min
Rf	Mass recovery of water to underflow
R_v	Volumetric recovery of feed slurry to underflow
α	Cyclone efficiency curve shape parameter (sharpness of separation)
β	Cyclone efficiency curve shape parameter (fishhook parameter)
θ	Full cone angle, degrees
λ	Hindered settling factor
ρ_p	Density of the cyclone feed pulp, g/cm^3
ρ_s	Density of the cyclone feed solids, g/cm^3

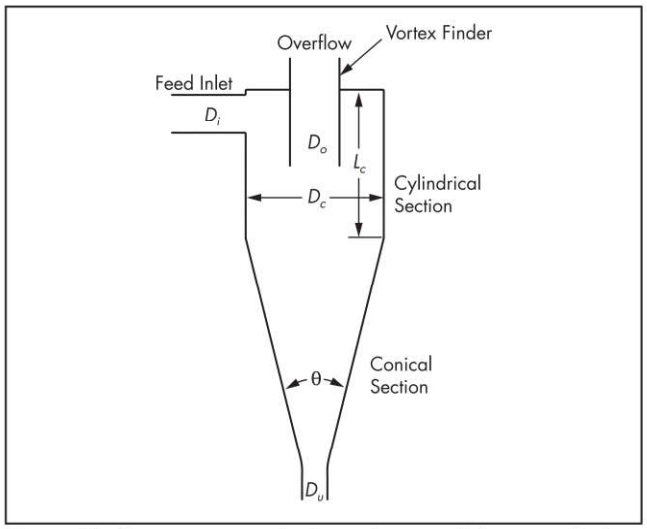

Figure 20 Nageswararao hydrocyclone model geometrical inputs

$$R_f = K_{w_o}\left\{D_c^{0.00}\right\}\left(\frac{D_o}{D_c}\right)^{-1.19}\left(\frac{D_u}{D_c}\right)^{2.40}\left(\frac{D_i}{D_c}\right)^{-0.50}\left(\frac{L_c}{D_c}\right)^{0.22}\theta^{-0.24}\left(\frac{P}{\rho_p g D_c}\right)^{-0.53}\lambda^{0.27} \quad \text{(EQ 12)}$$

$$R_v = K_{v_o}\left\{D_c^{0.00}\right\}\left(\frac{D_o}{D_c}\right)^{-0.94}\left(\frac{D_u}{D_c}\right)^{1.83}\left(\frac{D_i}{D_c}\right)^{-0.25}\left(\frac{L_c}{D_c}\right)^{0.22}\theta^{-0.24}\left(\frac{P}{\rho_p g D_c}\right)^{-0.31} \quad \text{(EQ 13)}$$

with the hindered settling factor, λ, defined as

$$\lambda = \frac{10^{1.82C_v}}{8.05 \times (1 - C_v)^2} \quad \text{(EQ 14)}$$

There are several points to be made regarding these correlations or model equations. The functional forms of the Nageswararao model equations were not determined via statistical approaches but rather selected based on the assumption that the effects of the independent operating variables followed a monomial power function relationship. In addition, each independent operating variable or factor was selected by the model developers based on phenomenological considerations (see Nageswararao et al. 2004 for amplification). This helps to explain the introduction of terms such as $(P/\rho_p g D_c)$ and λ, aimed at accounting for the centrifugal force field and hindered settling environment, respectively. The Nageswararao model also employs dimensionless variables for most of the hydrocyclone geometrical inputs, dividing each input by the diameter of the hydrocyclone, D_c. The model equations also contain four unique K values, K_{Qo}, K_{Do}, K_{Wo}, and K_{Vo}, or calibration parameters. These are material-dependent constants that allow the model to be tuned to particular feed materials, provided that measured plant data are available. In the absence of measured plant data, the model user is required to source appropriate K values from previous surveys or the literature. Because this has the potential to introduce significant error, the model predictions should be used with caution in any case of sourced K values (Nageswararao et al. 2004). To reiterate, this is one of the reasons that such empirical models are seldom directly used for hydrocyclone selection in greenfield process design.

With the $d50c$ and Rf values from the empirical model along with an α value fit to experimental data, the solids split to the underflow can be computed from the partition curve model given by

$$\hat{p}_i = Rf + (1 - Rf)\left[\frac{e^{\alpha\frac{d_i}{d50c}} - 1}{e^{\alpha\frac{d_i}{d50c}} + e^{\alpha} - 2}\right] \quad \text{(EQ 15)}$$

To quickly review, $\hat{p}_i$ is the predicted partition factor for size class i (fraction of feed in size class i reporting to the underflow) and d_i is the corresponding characteristic (*geomean*) size.

The Euler number, defined earlier, provides a means to predict the operating pressure of a hydrocyclone, given the feed flow rate and other relevant geometrical and operating inputs. In a brownfield project (i.e., K_{Qo} known with some confidence), this predicted operating pressure provides the necessary information for selecting the number of required hydrocyclones for a given condition while maintaining a practical operating pressure for hydrocyclone component wear and pumping power requirements. Within the Nageswararao model, the predicted operating pressure also serves as an input for the prediction of the dimensionless cut size, $d50c/D_c$, the recovery of water to underflow, Rf, and the volumetric recovery of feed slurry to underflow, R_v.

A weighted average of the direct prediction of Rf along with the indirect prediction of Rf from R_v allows for the determination of the water balance around the hydrocyclone, meeting the third requirement for a comprehensive prediction of hydrocyclone performance. It was noted by Nageswararao et al. (2004) that this weighted averaging procedure has been applied within the newer Nageswararao model. However, Nageswararao also notes that the direct model equation for Rf is a more accurate prediction and could be used independently. The volumetric recovery equation for R_v could then be considered superfluous in application of the model. Nageswararao notes that despite this, the volumetric recovery equation is unlikely to be removed from the newer version of the model as the existing parameter database is based on this described procedure. In the following example, the direct prediction of Rf is used in the analysis and R_v is disregarded.

An Example of Empirical Modeling

In Chapter 4.6, "Partition Curves," two data sets are presented for a survey on a ball mill–circuit grinding copper ore: one corresponding to a hard (*hypogene*) feed and the other to a soft (*supergene*) feed. These designations of *hard ore* and *soft ore* are retained here, again for consistency, although they could simply be considered as two independent survey campaigns on the same hydrocyclone cluster.

The general mass balanced test conditions for the hydrocyclone cluster for these two surveys are summarized in Table 3. In addition, the hydrocyclone geometry for both surveys is summarized in Table 4.

For both the hard ore and soft ore, Equation 15 was fit to the experimental partition factor results (from the mass balanced data). The results of this exercise are shown in Figure 21.

To assess the ability of the model to accurately predict hydrocyclone operation, the Nageswararao correlations were calibrated (i.e., K factors estimated) for the conditions of the hard ore survey. The resulting model, with the appropriate operating data, can then be applied to predict the soft ore survey results. A comparison between the actual soft ore survey results and these model-predicted results provides for a measure of the model accuracy, as shown in Table 5. (Note that in this table, the Rf value comes from the actual water split to the underflow stream, not from the particle size–based estimates in Figure 21.)

The model predictions for the soft ore survey have errors ranging from 3.8% to 12.6% relative to the observed experimental conditions. This error can be attributed to a range of factors, including model inaccuracy, experimental survey error, and any potential intrinsic changes in the ore characteristics between the two tests. When applying fitted K values from one survey to another operating condition, there is an inherent assumption that any ore-specific variables that could

Table 3 Mass balance in formation summary (hard and soft ore circuit surveys)*

Variable	Hard Ore Survey	Soft Ore Survey
Total feed flow rate, m^3/h	3,917	5,094
Number of hydrocyclones in operation	7	9
Operating pressure, kPa	98	97
Feed flow rate per hydrocyclone, m^3/h	560	566
Feed solids rate per hydrocyclone, t/h	442.0	591.2
Feed solids specific gravity, t/m^3	2.79	2.95
Feed percent solids by mass, %	52.4	61.8
Feed pulp density, t/m^3	1.507	1.690
Feed volume fraction of solids, v/v	0.283	0.354
Overflow solids rate per hydrocyclone, t/h	105.4	144.2
Overflow percent solids by mass, %	29.5	41.1
Underflow solids rate per hydrocyclone, t/h	336.6	446.9
Underflow percent solids by mass, %	69.2	73.7

*See Chapter 4.6, "Partition Curves."

Table 4 Hydrocyclone geometry variables for the surveys

Symbol	Description	Value
D_c	Hydrocyclone diameter, m	0.660
L_c	Cylinder length, m	0.932
D_i	Equivalent inlet diameter, m	0.272
D_o	Vortex finder diameter, m	0.254
D_u	Apex diameter, m	0.178
θ	Cone angle, degrees	22
G	Gravitational acceleration, m/s^2	9.81

influence the hydrocyclone (such as clay content or particle size distribution) are remaining relatively constant. In this particular example, there is certainly room for these kinds of errors, given the markedly different ores.

To illustrate the kind of optimization work that can be undertaken, the following example looks at a change in the hydrocyclone apex diameter—one calculated to reduce the rather large water-based *Rf* value observed in the survey. (Because hydrocyclones are most often used in closed circuits, one must look at the whole system and not just the hydrocyclone. However, for illustrative purposes, the authors look only at the hydrocyclone in this example.) Based on the cursory evaluation, a simulated case can be completed with an adjustment from the existing 178-mm apex diameter to a 152-mm apex diameter. The feed pressure, slurry conditions, and all other hydrocyclone geometry variables were held constant. The results of this evaluation are shown in Table 6 and in Figure 22. It is quite clear that the reduction in apex diameter has a notable change in the predicted cut size and water bypass. These changes have a significant effect on the partition curve, as shown in Figure 22.

Summary

Empirical hydrocyclone models, such as Nageswararao's, are quite commonly used in simulation studies for grinding circuits. They are reasonably accurate when used in process analysis or optimization work, as they can be calibrated to plant survey data. However, the material-related constants (the *K* values) clearly vary over a substantial range, which limits model applicability in process design. That said, most hydrocyclone OEMs use these models as a decision support tool in equipment selection.

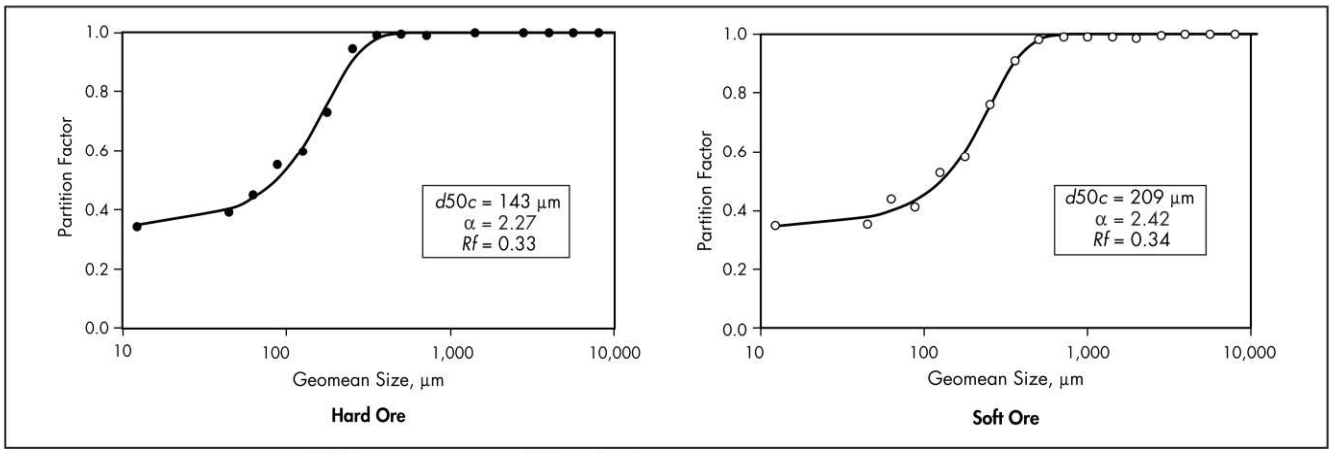

Figure 21 Partition curve model fit to experimental data for the two surveys

Table 5 Calibration of the Nageswararao model to the hard ore data and prediction of the soft ore parameters

	Hard Ore Survey			Soft Ore Survey		
Variable	Experimental	Model Fit	Fitted K Values	Experimental	Model Prediction	Error, %
Feed flow rate, *Q*	560	560	K_{Qo} = 554	566	526	–7.1%
Cut size, *d50c*	143	143	K_{Do} = 0.000114	209	235	12.6%
Actual water bypass, *Rf*	0.37	0.37	K_{Wo} = 12.466	0.44	0.45	3.8%

Table 6 Exploring a change in apex diameter for the hard ore case

Variable	Hard Ore Survey			Simulated Case, 152-mm Apex—Model Prediction
	Experimental	Model Fit	Fitted K Values	
Feed flow rate, *Q*	560	560	K_{Qo} = 554	560
Cut size, *d*50*c*	143	143	K_{Do} = 0.000114	154
Actual water bypass, *Rf*	0.37	0.37	K_{Wo} = 12.466	0.25

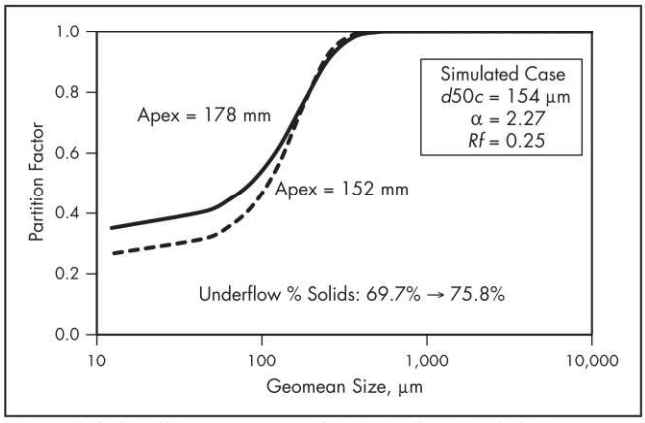

Figure 22 Partition curve predicted for the simulated case, 152-mm apex

PROCESS CONTROL

Equations 10–12 indicate that real-time hydrocyclone performance depends on two operational variables: flow (or pressure) and hydrocyclone feed density (percent solids). To the extent these variables can be modulated, they can be embedded in process control schemes.

Looking just at open-circuit operation, and using the hard ore hydrocyclone data and model, the predicted variations of the hydrocyclone overflow P80 with variations in hydrocyclone feed density and the hydrocyclone feed pressure (or flow) are shown in Figure 23. Keeping the vertical axes scales the same illustrates that the feed percent solids has a larger impact on overflow particle size than does pressure (or flow) over the normal ranges of variation.

In many cases, the feed flow rate to the hydrocyclone varies, and over a broad range. One operating tactic that is frequently employed is to regulate hydrocyclone pressure; that is, to keep it low enough to reduce wear and high enough to preserve stable operation and even influence the overflow particle size distribution. Provided that the hydrocyclones are fit with automatic gate valves, which are integrated into the process control system, this can be automated by opening or closing hydrocyclones. To prevent *chatter*, once a hydrocyclone is opened or closed, it is common to suspend any further changes in hydrocyclone operating status for a suitable length of time (e.g., 15 minutes or more). Figure 24 illustrates the variation of operating pressure and overflow particle size for a given feed flow, where the number of operating hydrocyclones is varied. As expected, pressure is very dependent on the number of hydrocyclones running, but as was seen in the previous figure, hydrocyclone overflow size is not.

Probably the most common application of hydrocyclones in mineral processing applications is in closed-circuit grinding, and a typical ball mill–hydrocyclone subcircuit is illustrated in Figure 25. While the open-circuit results still apply, the closed circuit complicates process control. Choosing the regulatory control structure (i.e., pairing controlled and manipulated variables in the proportional–integral–derivative [PID] controller loops) has been the subject of some debate over the years, but the industry appears to have converged on a best practice.

To amplify, consider the example shown in Figure 26. Here, a relatively small grinding circuit (treating ~325 metric tons per hour [t/h] of fresh feed) was subjected to a small step increase (~7.5%) in the pump box water flow, and the dynamic responses of hydrocyclone feed density, hydrocyclone overflow particle size, and hydrocyclone overflow density were recorded. (The numerical scale for the hydrocyclone overflow density was also missing in the original publication.) The initial effect of the water is to reduce all three variables. However, with a finer cut size, the recirculating load and hydrocyclone underflow percent solids both increase, which acts to increase the hydrocyclone feed density and overflow

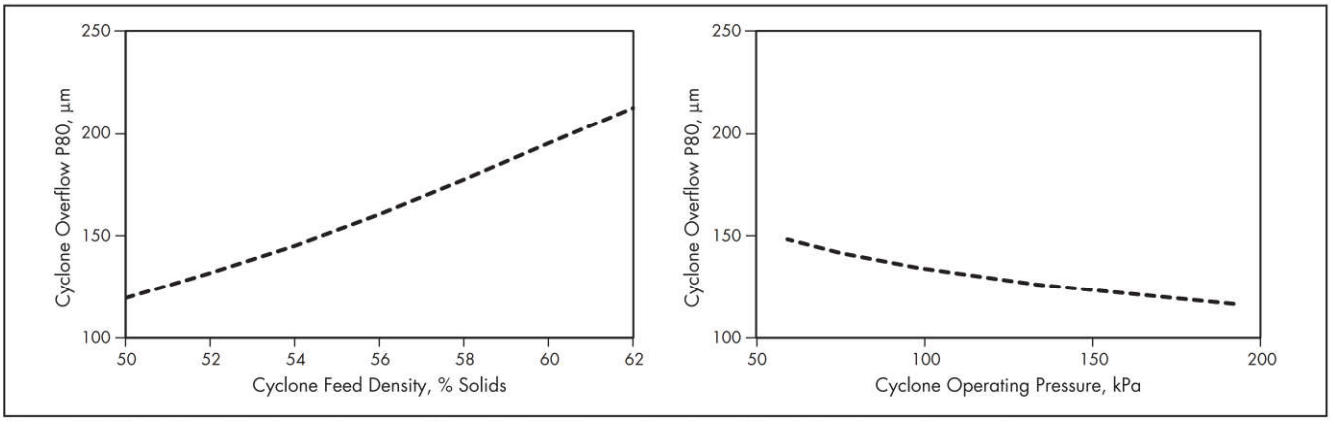

Figure 23 Variation of hydrocyclone overflow size (P80) as a function of feed density and operating pressure

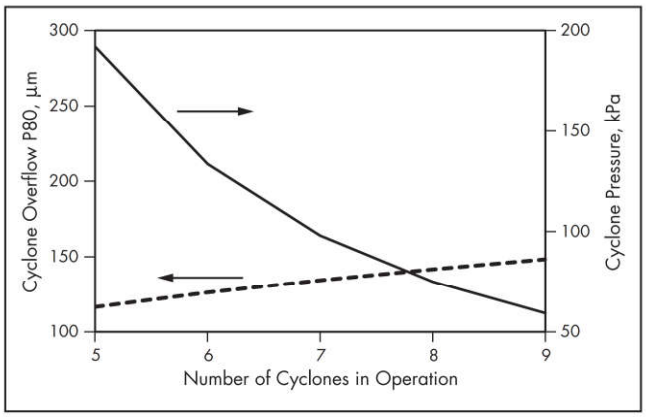

Figure 24 Variation of hydrocyclone overflow size (P80) and operating pressure as a function of the number of hydrocyclones running

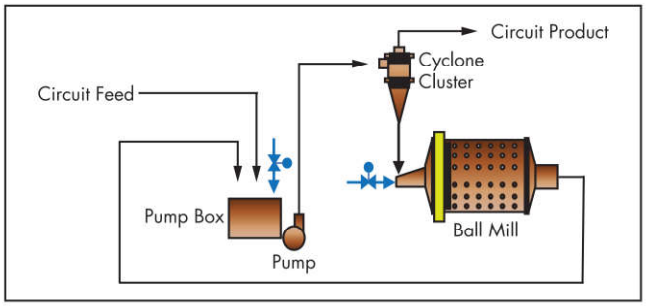

Figure 25 Typical ball mill–hydrocyclone subcircuit flow sheet

particle size. In the end, the variable most affected is the hydrocyclone overflow density, while the other two return almost to the original levels. This example is intended simply to illustrate some of the challenges with hydrocyclone performance management in closed-circuit operation.

Returning to best practice, the typical pairing is illustrated in the process matrix shown in Figure 27. The entries define the response of a controlled variable to an increase in a manipulated variable in terms of speed and direction. (Here the entries define the response of a controlled variable to an increase in a manipulated variable speed: fast, slow, and none; and the direction: + for increase and – for decrease.) The shaded boxes indicate the preferred pairings, keeping in mind that regulating hydrocyclone feed density may only be practical for rejecting shorter-term (e.g., periods of 10–15 minutes or less) disturbances.

		Controlled		
	Process Matrix	Cyclone Feed Density	Pump Box Level	Cyclone Pressure
Manipulated	Pump Box Water	– Fast	+ Fast	None
	Pump Speed	None	– Fast	+ Fast
	No. of Cyclones	None	None	– Fast

Direction: + Increase, – Decrease

Figure 27 Process matrix for regulatory loop pairing for the subcircuit in Figure 25

RECENT DEVELOPMENTS

Design Enhancement on Existing Hydrocyclones

During the past 15 years, new and more efficient hydrocyclone designs have been introduced. Design improvements were apparently made in the feed inlet to minimize turbulence when the new feed enters the body of the hydrocyclone, which impacts capacity, wear, and efficiency. Moreover, changes to the hydrocyclone body design were also made. As shown in Figure 28, the potential for efficiency improvements associated with increasing residence time in the critical conical section of the hydrocyclone has been exploited. An extensive redesign campaign yielded optimal combinations of cylinder and cone length, as well as cone design for each standard hydrocyclone diameter.

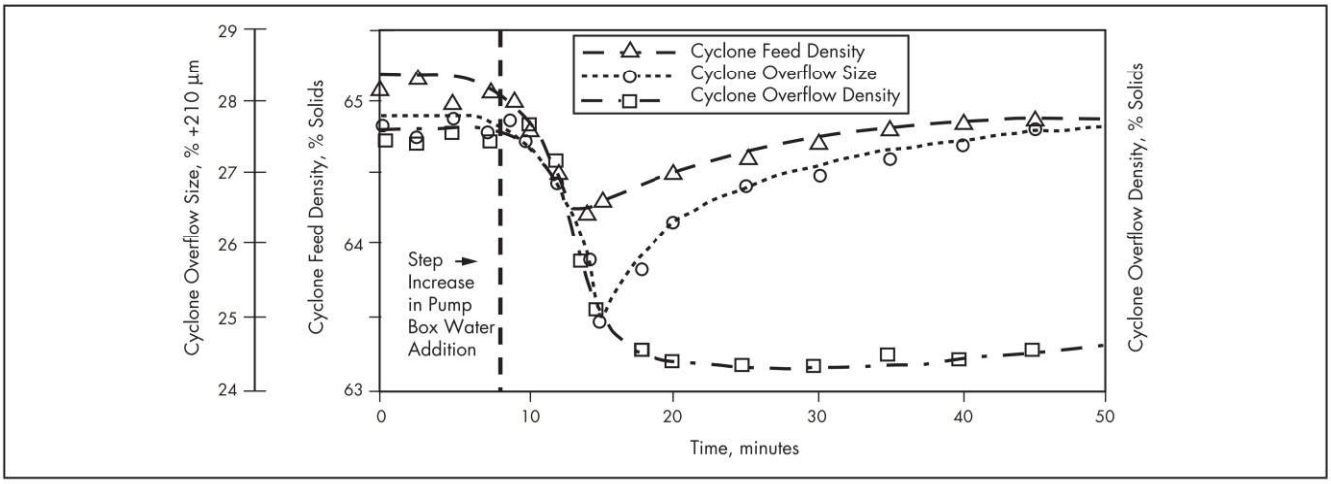

Source: Bradburn et al. 1977

Figure 26 Response of a loaded ball mill–cyclone circuit to a step change of 100 U.S. gallons per minute in pump box water

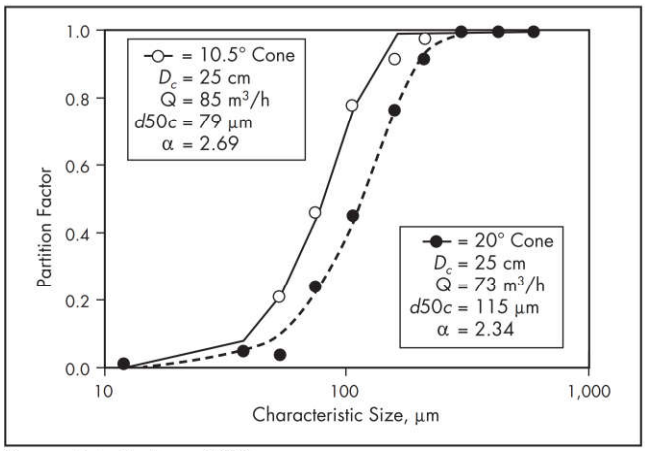

Source: Krebs Engineers 2000

Figure 28 Effect of cone angle on hydrocyclone performance

Mohanty et al. (2002) reported that a conventional hydrocyclone separating a fine coal feed (~45 µm cut target) yielded an efficiency of R_u = 37% (efficiency of fines removal from the feed), while the new design improved this to 68%. Adding an attachment, which offers a means of injecting water into the lower cone section of a hydrocyclone to remove fines, gave a further increase to 70%.

New Hydrocyclone Systems

In addition to the work underway to improve traditional hydrocyclone designs, new designs are also under study by OEMs and researchers alike, although in general, these are application-specific products.

Briefly, one new hydrocyclone design (see Mainza et al. 2004) is intended for use in applications where there are components of distinctly different densities. In conventional hydrocyclones, the heavier minerals concentrate near the hydrocyclone wall, which creates a heavy medium that selectively sends the larger, lighter particles toward the inside of the hydrocyclone where they can be sent to the overflow. In the case of the platinum ores in South Africa, the lighter silica gangue contain the platinum group metals, while the heavier chromite is barren. Larger silica particles that report to the overflow represent potential recovery losses in the flotation process. The new hydrocyclone design uses concentric vortex finders to produce two overflow products. The inner vortex finder collects the fine particles, which are sent directly to flotation. The outer vortex finder collects a coarser middlings overflow, rich in coarse silica, which is then screened to ensure that the coarser material gets to the mill for further grinding, while the finer heavy material joins the flotation feed. Development work continues with this system, which would appear to have other applications in the mineral processing industry.

Another new hydrocyclone design (Castro et al. 2009), which employs two-stage classification as a means to reduce *Rf* and increase α, has been a concept studied and promoted by many academics and a few operators. It does find application in some coal and iron ore flow sheets, but generally, the extra footprint and the capital and operating expenses associated with such an approach have diminished interest among plant designers. One area where this has been extensively applied is in tailings dam construction, where it is critically important to remove as much of the fines as possible from the sand product used to construct the dam. In these cases, two batteries of hydrocyclones (larger primaries followed by smaller secondaries) are common, to ensure that sand percolation rates are sufficiently high to avoid stability problems in the dam. This particular design performs these steps in a single unit.

Figure 29 is an illustration of the two-stage classification unit, and Figure 30 presents partition curves for the primary and secondary units and the overall curve. Note the adjustment system on the primary underflow, which acts conceptually like a variable apex. The effects on *Rf* and hence fine-particle content in the underflow are clear. All of the case studies reported by Castro et al. (2009) are on tailings; however, one can easily envisage other applications.

Instrumentation

Although little has been published thus far, the major hydrocyclone suppliers and some third parties are actively looking at technology value additions that will help improve performance and minimize maintenance costs. For example,

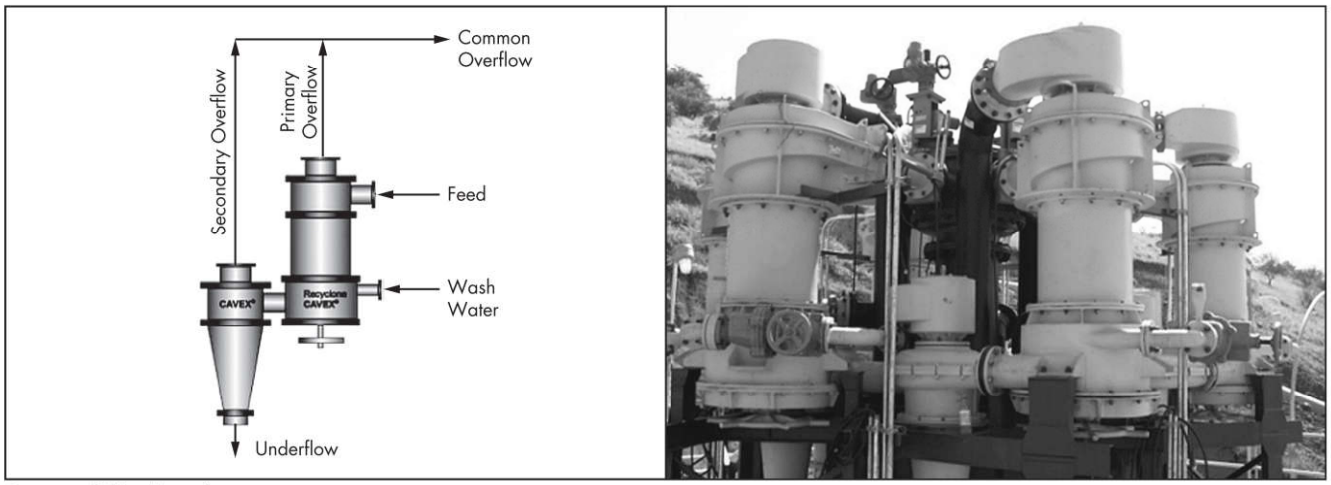

Courtesy of Weir Minerals

Figure 29 Schematic and installation of the two-stage classification unit

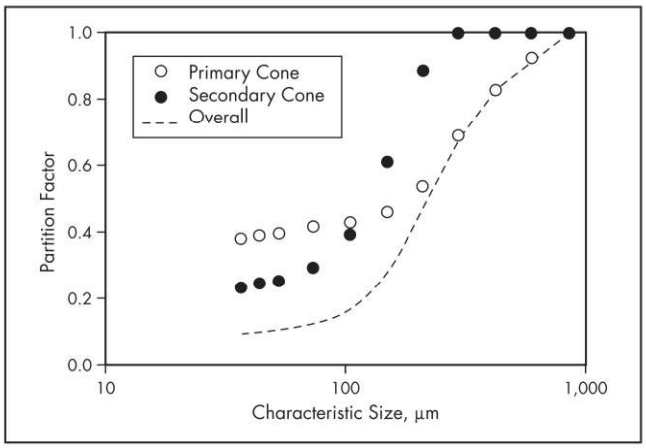

Adapted from Castro et al. 2009

Figure 30 Partition curves for a two-stage classification unit

Table 7 Hydrocyclone lining materials

Rubber	Ceramics
BPC (premium natural rubber)	CR (nitride-bonded silicon carbide)
Polyurethanes	CX (reaction-bonded silicon carbide)
Neoprene	CZ (sintered alpha silicon carbide)
Other synthetics and blends	

Courtesy of FLSmidth–Krebs

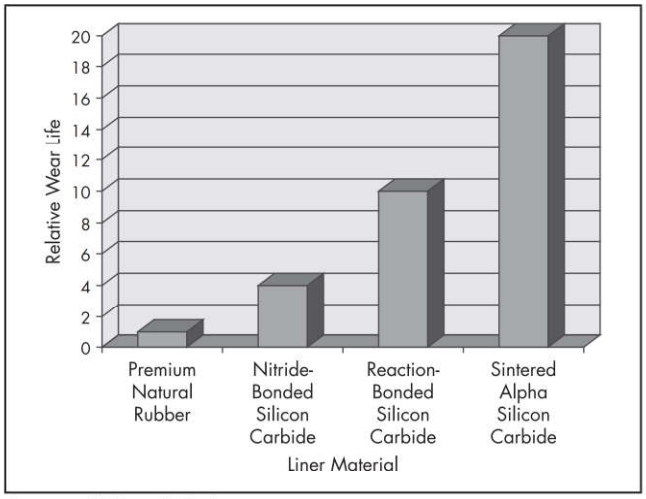

Courtesy of FLSmidth–Krebs

Figure 31 Relative wear life of the more common hydrocyclone lining materials

hydrocyclones are known to vibrate when they transition from normal underflow spray to roping regime, and vibration and/or acoustics (e.g., Wedeles 2007) could be applied to diagnose this event or other events such as apex plugging (e.g., tramp grinding balls in hydrocyclone feed). More recently, an acoustic sensor (Cirulis and Russell 2011) and a vibration application for incident detection (Moore 2016) have been developed. Another area also under study by pump manufacturers is the elusive measurement of the relative wear of hydrocyclone liners. The interested reader should contact suppliers directly on this topic.

Computational Fluid Dynamics

As was seen earlier in the discussion on screens, most major suppliers are rapidly embracing sophisticated simulation tools as way to create and screen virtual machines for the purposes of design and optimization. While this does not preclude the necessary step of field testing prototypes, it does help in the selection of the most appropriate candidate designs, reducing research and design costs and technical risk, and shortening the time to market.

Computational fluid dynamics (CFD) is the simulation technique of choice for fluid systems such as the hydrocyclone. At this stage, however, it is impossible to simulate real slurries, and the standard approach is to simulate the fluid, and then to use these results with some *tracer particles* (within CFD or in the discrete element modeling environment) to gain insight on classification efficiency. This one-way coupling (the fluid influences the particles, but the converse is not true), albeit with dilute suspensions, gives insights into classification efficiency.

Suffice to say, CFD played a major role in the development of new and more efficient hydrocyclone designs and the two-stage classification unit described earlier. For the interested reader, the article by Delgadillo and Rajamani (2007) provides a vision of the benefits of CFD in advancing the hydrocyclone state of the art.

Wear Lining Materials

Wear lining materials is a very important topic for plant operators who need to minimize operating costs and downtime and optimize maintenance cycles. Because hydrocyclones are usually operated in a cluster, the *cassette maintenance model*, which is to close and remove a hydrocyclone for a rebuild and replace that unit with a new or rebuilt one, is considered best practice.

Briefly, hydrocyclones are usually constructed of polyurethane or steel, and less often with other materials, for example, composites. Smaller hydrocyclones, say D_c less than 100–150 mm, are frequently polyurethane, while the larger ones, more common in mining applications, are more typically fabricated from steel or composites. From a wear parts perspective, polyurethane units are usually operated until the end of their service life, and then replaced with a new hydrocyclone.

Conversely, steel or composite hydrocyclones are designed with external housings and lined with wear-resistant materials, such as natural rubber, polyurethane, or ceramics, as summarized in Table 7. The relative wear life of the more common linings is illustrated in Figure 31, and as would be expected, cost is proportional to the service life.

Natural rubber is generally cheaper than polyurethane, and the two typically have similar wear characteristics; consequently, rubber lining is in more common usage. An exception may arise when, for example, the chemical environment (e.g., fuel oils) dictates against natural rubber. Ceramics are the most expensive lining option but offer the best wear resistance.

The challenge is to develop a cost-effective lining solution that essentially ensures that all parts of the lining wear out at about the same time. This is complicated because the wear rates generally vary depending on the location in the hydrocyclone; for example, in order of wear rate, first the apex, then the lower cone, then middle cone, then inlet. To illustrate with an example, one OEM, working closely with a major

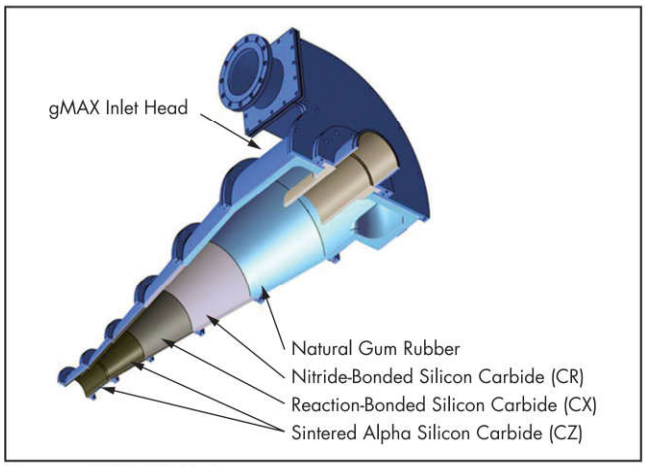

Courtesy of FLSmidth–Krebs

Figure 32 Using multiple lining materials to optimize service life and minimize cost

customer, was able to move from fully rubber-lined hydrocyclones, with an average operating lifetime of 4,000 hours, to the new more efficient hydrocyclones, using a combination of linings, as shown in Figure 32, to achieve average operating lifetimes of 13,000 hours. The upper regions of the hydrocyclone (inlet head, cover plate, and upper conical regions) are lined with rubber, and the lower portions of the hydrocyclone are lined with ceramics, progressing to longer wear-life components as the wear rate increases. Again, the OEM is in a very good position to provide expert application advice on wear liner choices.

ACKNOWLEDGMENTS

The authors extend their most sincere thanks to Weir Minerals, FLSmidth–Krebs, and the many colleagues in Metso Mining who provided much of the information contained herein, as well as some very helpful feedback.

REFERENCES

Aldrich, C. 2015. Hydrocyclones. In *Progress in Filtration and Separation*. Edited by S. Tarleton. London, UK: Elsevier. pp. 1–24.

Arterburn, R. 1982. The sizing and selection of hydrocyclones. In *Design and Installation of Comminution Circuits*. Edited by A. Mular and G.V. Jergensen. Littleton, CO: SME-AIME. pp. 592–607.

Asomah, I., and Napier-Munn, T. 1997. An empirical model of hydrocyclones incorporating angle of cyclone inclination. *Miner. Eng.* 10(3):339–347.

Bradburn, R., Flintoff, B., and Walker, R. 1977. Practical approach to digital control of a grinding circuit at Brenda Mines Ltd. *Trans. SME* 262(7):140–147.

Bradley, D. 1965. *The Hydrocyclone*. New York: Pergamon Press.

Castro, E., Lopez, J., and Switzer, D. 2009. Maximum classification efficiency through double classification using the ReCylone. In *Recent Advances in Mineral Processing Plant Design*. Edited by D. Malhotra, P. Taylor, E. Spiller, and M. LeVier. Littleton, CO: SME. pp. 444–454.

Cirulis, D., and Russell, J. 2011. CiDRA CYCLONEtrac at Kennecottt Utah Copper. Presented at the *Engineering and Mining Journal* (E&MJ) Mineral Processing Conference, Lake Tahoe, NV, October 10–12.

Delgadillo, J., and Rajamani, K. 2007. Exploration of hydrocyclone designs using computational fluid dynamics. *Int. J. Miner. Proc.* 84(1-4):252–261.

Flintoff, B., and Kuehl II, R. 2011. Classification by screens and cyclones. In *SME Mining Engineering Handbook*, Vol. 2. Edited by P. Darling. Englewood, CO: SME.

Flintoff, B., Plitt, L.R., and Turak, A. 1987. Cyclone modeling: A review of present technology. *CIM Bull.* 80(September):39–50.

JKTech. 2014. *JKSimMet User Manual*, Version 6.0. Brisbane, Queensland: JKTech Pty Ltd.

Kelly, E.G., and Spottiswood, D.J. 1982. *Introduction to Mineral Processing*. Hoboken, NJ: John Wiley and Sons.

Krebs Engineers. 2000. *Krebs gMAX Cyclones—For Finer Separations with Larger Diameter Cyclones*. www.krebs.com.

Mainza, A., Powell, M., and Knopjes, B. 2004. A comparison of different cyclones in addressing challenges in the classification of the dual density UG2 platinum ores. In *International Platinum Conference: "Platinum Adding Value."* Johannesburg: Southern African Institute of Mining and Metallurgy. pp. 341–348.

Mohanty, M., Palit, A., and Dube, B. 2002. A comparative evaluation of new fine particle separation technologies. *Miner. Eng.* 15(10):727–736.

Moore, E. 2016. All sorted out: A new cyclone diagnostic system is keeping things moving at Copper Mountain. *CIM Mag*. www.cim.org/en/Publications-and-Technical-Resources/Publications/CIM-Magazine/2016/February/upfront/All-sorted-out.aspx.

Nageswararao, K., Wiseman, D., and Napier-Munn, T. 2004. Two empirical hydrocyclone models revisited. *Miner. Eng.* 17:671–687.

Narasimha, M., Mainza, A., Holtham, P., Powell, M., and Brennan, M. 2014. A semi-mechanistic model of hydrocyclones: Developed from industrial data and inputs from CFD. *Int. J. Miner. Process.* 133:1–12.

Olson, T., and Turner, P. 2002. Hydrocyclone selection for plant design. In *Mineral Processing Plant Design, Practice, and Control*, Vol. 1. Edited by A.L. Mular, D.N. Halbe, and D.J. Barratt. Littleton, CO: SME. pp. 880–893.

Plitt, L.R., Flintoff, B., and Stuffco, T. 1987. Roping in hydrocyclones. In *Proceedings of the 3rd International Conference on Hydrocyclones*. Edited by P.A. Wood. London: BHRA/Elsevier. pp. 21–33.

Renner, V., and Cohen, H. 1978. Measurement and the interpretation of size distributions within a cyclone. *Trans. Inst. Chem. Eng.* 87:C139–C145.

Schmidt, M., and Turner, P. 1993. Flat bottomed or horizontal cyclones: Which is right for your world? *World. Min. Equip.* pp. 151–152.

Svarovsky, L. 2000. *Solids–Liquid Separation*, 4th ed. Boston: Butterworth-Heinemann.

Wedeles, M. 2007. Smart cyclone: A tool for optimizing cyclone operation. Presented at SAG 2007, Vina del Mar, Chile.